

Obtaining accurate mean velocity measurements in high Reynolds number turbulent boundary layers using Pitot tubes

S. C. C. Bailey^{1,†}, M. Hultmark², J. P. Monty³, P. H. Alfredsson⁴,
M. S. Chong³, R. D. Duncan⁵, J. H. M. Fransson⁴, N. Hutchins³, I. Marusic³,
B. J. McKeon⁶, H. M. Nagib⁵, R. Örlü⁴, A. Segalini^{4,7}, A. J. Smits²
and R. Vinuesa⁵

¹Department of Mechanical Engineering, University of Kentucky, Lexington, KY 40506, USA

²Department of Mechanical and Aerospace Engineering, Princeton University, Princeton, NJ 08544, USA

³Department of Mechanical Engineering, The University of Melbourne, Victoria 3010, Australia

⁴Linné FLOW Centre, KTH Mechanics, SE-100 44 Stockholm, Sweden

⁵Illinois Institute of Technology, Chicago, IL 60616, USA

⁶Graduate Aeronautical Laboratories, California Institute of Technology, Pasadena, CA 91125, USA

⁷II Facoltà di Ingegneria, Università di Bologna, I-47100 Forlì, Italy

(Received 5 March 2012; revised 31 August 2012; accepted 27 October 2012)

This article reports on one component of a larger study on measurement of the zero-pressure-gradient turbulent flat plate boundary layer, in which a detailed investigation was conducted of the suite of corrections required for mean velocity measurements performed using Pitot tubes. In particular, the corrections for velocity shear across the tube and for blockage effects which occur when the tube is in close proximity to the wall were investigated using measurements from Pitot tubes of five different diameters, in two different facilities, and at five different Reynolds numbers ranging from $Re_\theta = 11\,100$ to 67 000. Only small differences were found amongst commonly used corrections for velocity shear, but improvements were found for existing near-wall proximity corrections. Corrections for the nonlinear averaging of the velocity fluctuations were also investigated, and the results compared to hot-wire data taken as part of the same measurement campaign. The streamwise turbulence-intensity correction was found to be of comparable magnitude to that of the shear correction, and found to bring the hot-wire and Pitot results into closer agreement when applied to the data, along with the other corrections discussed and refined here.

Key words: turbulent boundary layers, turbulent flows

1. Introduction

To measure the mean velocity in a turbulent wall-bounded flow, it is common to use either Pitot tubes or hot-wire probes. Pitot tubes require corrections for shear and near-wall effects, and possibly for the effects of turbulence and low Reynolds numbers. Hot-wires need to be calibrated (typically by reference to a Pitot or Pitot-static tube),

[†] Email address for correspondence: sca Bailey@engr.uky.EDU

and the measurements can be affected by heat conduction to the walls, free convection effects, ambient temperature changes, calibration drift, the difficulty of determining the precise wall position, and other flow-dependent influences. It is not surprising, therefore, that hot-wire and Pitot tube measurements of the mean velocity profile do not always agree, especially in the near-wall region. McKeon *et al.* (2003) illustrated this problem by comparing some recent near-wall studies of pipe flow, and found discrepancies up to 15 % among the data at $y^+ = 20$, where $y^+ = yu_\tau/\nu$, and y is the distance from the wall, $u_\tau = \sqrt{\tau_w/\rho}$, τ_w is the wall shear stress, and ρ and ν are the fluid density and kinematic viscosity, respectively. The main candidates for this discrepancy include the inaccuracy in finding the wall position (Örlü, Fransson & Alfredsson 2010) and the uncertainty in u_τ , although a recent investigation by Örlü & Alfredsson (2010) revealed that the mean velocity measured by hot-wire probes can also be susceptible to spatial filtering effects, which were previously thought to be confined to measurements of turbulence (cf. Ligrani & Bradshaw 1987).

In recent studies of the mean flow, there seems to have been a tendency to favour the hot-wire over the Pitot tube. For example, all mean velocity profiles reported in the studies by Hites (1997), Österlund (1999), Hutchins & Marusic (2007), Nickels *et al.* (2007) were obtained using single, normal hot-wires. Certainly, if the principal aim is to acquire turbulence data, the hot-wire will give a measure of the mean velocity without any additional work, and the hot-wire may be able to approach the wall more closely than a conventional Pitot tube. In addition, the corrections required to obtain accurate Pitot tube measurements give the impression that Pitot tubes are a somewhat unreliable device, especially in regions near the wall where all the corrections may become important at the same time. However, given the difficulty in eliminating sources of error in hot-wire measurements, and given that a Pitot tube can be in contact with the wall at the initialization of the measurement thus providing a fixed reference distance to the wall, it is not clear whether hot-wire probes provide any accuracy advantage over Pitot tubes when measuring mean velocity in wall-bounded flows.

In 2008, researchers from Caltech, Illinois Institute of Technology (IIT), the Royal Institute of Technology (KTH), University of Bologna, Shinshu University, Nagoya University, the University of Melbourne and Princeton University undertook a cooperative experimental effort called the International Collaboration on Experimental Turbulence (ICET) with the aim of studying methods and facilities used in the study of wall-bounded turbulent flows, with a particular emphasis on high Reynolds number turbulent boundary layers.

Three facilities capable of providing moderate to high Reynolds number boundary layers were used: the minimum turbulence level (MTL) wind tunnel at KTH, the high Reynolds number boundary layer wind tunnel (HRNBLWT) at the University of Melbourne, and the National Diagnostic Facility (NDF) at IIT. Measurements in these facilities were performed over a range of Reynolds numbers based on momentum thickness, Re_θ , from 11 000 to 67 000. By using a number of different measurement techniques, the ICET team proposed to compare nominally identical flows generated in three different facilities. As one part of this effort, a wide range of Pitot measurements were taken in the MTL and HRNBLWT, and it is these measurements that are of concern here.

Here we describe the accuracy of Pitot tube measurements and the attendant suite of correction procedures. We aim to establish definitively that Pitot tubes, when used carefully, can give reliable data with a very low level of uncertainty in the mean velocity and the effective position of the tube through comparison with mean hot-wire

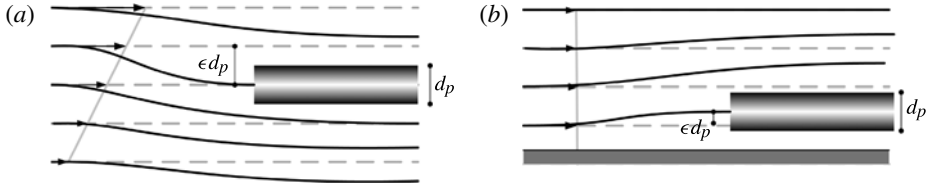


FIGURE 1. Illustration of effect of Pitot tube on streamlines: (a) in velocity shear and (b) near a solid boundary. Adapted from McKeon *et al.* (2003).

data from the same measurement campaign. There, the complete data set will be used to evaluate the integral properties of the boundary layer and their Reynolds number dependence, the extent of the logarithmic part of the profile, and the uncertainty in estimating the log-law constants.

2. Pitot tube corrections

To obtain accurate velocity measurements in a boundary layer using a Pitot tube, certain corrections need to be applied (Tavoularis 2005; McKeon 2007). McKeon *et al.* (2003) identified a low Reynolds number correction (also called the viscous correction), a shear correction (otherwise known as the velocity gradient correction), a near-wall correction, a turbulence correction, and, if the static pressure is measured using a wall tapping, a Reynolds-number-dependent correction for the static pressure reading may be necessary. For the experiments reported here the static tap correction was found to be unnecessary, since the tap diameter remained sufficiently small relative to the viscous scale in all cases; see McKeon & Smits (2002) for a static tap correction used in high Reynolds number pipe flow.

For the viscous correction, experimental results indicate that viscous effects can be ignored for $Re_d > 100$, where the tube Reynolds number Re_d is based on local mean velocity U and Pitot tube outer diameter d_p (MacMillan 1954; Chue 1975). For $30 < Re_d < 100$, Zagarola & Smits (1998) suggested that the correction for the viscous effects could be represented by

$$\frac{\Delta P}{\frac{1}{2}\rho U^2} = 1 + \frac{10}{Re_d^{1.5}}, \quad (2.1)$$

where ΔP is the measured difference between total and static pressure.

Use of a Pitot tube in a shear flow introduces additional adverse effects through nonlinear averaging of the pressure variation across the probe face and asymmetric deflection of the streamlines. The effect of spatial averaging across the face of the probe is usually small compared to that of asymmetric streamline deflection, thus a velocity gradient correction typically only compensates for the higher velocity streamlines deflecting towards the tube, as illustrated in figure 1(a). As a result, the measured total pressure at the tube position is larger than the pressure would be without the tube in place. The most common correction for this effect is to apply a virtual shift to the location of the measurement tube in the higher velocity direction by an amount Δy , where

$$\Delta y = \epsilon d_p, \quad (2.2)$$

thereby compensating for the streamline deflection. MacMillan (1957) proposed a constant value of $\epsilon = 0.15$, while other authors have found $0.15 < \epsilon < 0.19$ (see, for example, Tavoularis & Szymczak 1989). Citing earlier theoretical work by Hall (1956) and Lighthill (1957), McKeon *et al.* (2003) introduced a correction that links ϵ to the local velocity gradient through

$$\epsilon = 0.15 \tanh(4\sqrt{\alpha}), \quad (2.3)$$

where α is a non-dimensional velocity gradient given by

$$\alpha = \frac{d_p}{2U} \frac{dU}{dy}. \quad (2.4)$$

This correction asymptotes to the MacMillan value of ϵ in strong velocity gradients and it has the advantage that it gives $\epsilon = 0$ in uniform flow.

A near-wall correction is required to compensate for additional blockage effects in the vicinity of a solid boundary, whereby the blockage of the tube causes a reduction in the shear-induced streamline deflection, as illustrated in figure 1(b). MacMillan (1957) found this effect to be important within two tube diameters of the wall, and suggested that, in addition to the shear correction given by (2.2), the velocity in this region should be increased by the amount ΔU , where

$$\frac{\Delta U}{U} = 0.015e^{-3.5(y/d_p - 0.5)}. \quad (2.5)$$

MacMillan (1957) noted that this correction should only be used for $30 < d^+ < 230$ where $d^+ = d_p u_\tau / \nu$. McKeon *et al.* (2003) proposed an alternative near-wall correction method based on the Preston tube results of Patel (1965), which were obtained in various wall-bounded flows, and suggested that for $y/d_p < 2$, (2.3) for ϵ should be replaced by

$$\epsilon = \begin{cases} 0.150 & \text{for } d^+ < 8, \\ 0.120 & \text{for } 8 < d^+ < 110, \\ 0.085 & \text{for } 110 < d^+ < 1600. \end{cases} \quad (2.6)$$

A turbulence correction may also be necessary, although the magnitude and form of the turbulence correction for Pitot tube measurements continues to be a matter of debate, particularly in light of the Pitot tube measurements in high Reynolds number turbulent pipe flow reported by Zagarola & Smits (1998) and subsequent re-analysis by Perry, Hafez & Chong (2001). In essence, the unsteadiness introduced by turbulence increases the measured total pressure. Goldstein (1938) investigated the effects of turbulence theoretically and suggested that

$$\Delta P = \frac{1}{2} \rho (U^2 + \overline{u'^2} + \overline{v'^2} + \overline{w'^2}), \quad (2.7)$$

where $\overline{u'^2}$, $\overline{v'^2}$ and $\overline{w'^2}$ are the three components of the turbulence intensity (using the coordinate system considered here, these components are taken to be in the streamwise, wall-normal, and cross-stream directions, respectively). This dependence can be written as

$$\Delta P = \frac{1}{2} \rho (U^2 + \varphi \overline{u'^2}), \quad (2.8)$$

where φ accounts for the effects of anisotropy and integral length scale of the turbulence (Tavoularis 2005). Note that in a boundary layer the near-wall turbulence

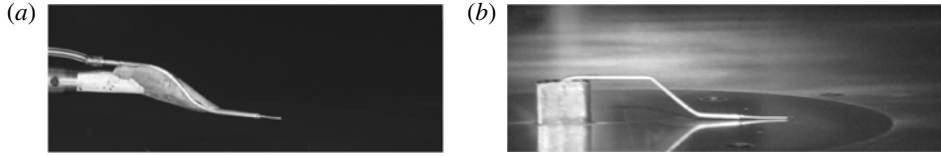


FIGURE 2. The two tube support structures used in this study: (a) McKeon *et al.* design; and (b) new support structure.

is highly anisotropic with the degree of anisotropy varying throughout the wall layer, so that φ will be a nonlinear function of y . Many other turbulence corrections have been proposed (see, for example, Ozarapoglu 1973 and Dickinson 1975), but no single correction has been found to work satisfactorily in all conditions. Pitot tube vibration can potentially introduce effects similar to that of turbulence, but in turbulent wall-bounded flows these effects are usually small when compared to that of the turbulence itself. One of the aims of the current work is to more closely examine the influence of the turbulence on the mean velocity measured using a Pitot tube.

3. Experiment description

3.1. Experimental facilities

Detailed Pitot tube measurements were conducted in two of the three ICET wind tunnel facilities: in May 2008 in the MTL wind tunnel at KTH, Stockholm, Sweden (described in detail by Lindgren & Johansson 2002), and in August 2008 in the High Reynolds Number Turbulent Boundary Layer Wind Tunnel (HRNBLWT) at the University of Melbourne, Australia (as described by Nickels *et al.* 2007). In the MTL, the boundary layer developed along a plate located at the wind tunnel mid-plane, as described by Österlund (1999) but with a different trailing edge flap angle and boundary layer trip. In the HRNBLWT, the boundary layer developed along the tunnel floor, as described by Nickels *et al.* (2007).

3.2. Instrumentation: Pitot tube measurements

In the MTL, Pitot tubes were used with four different outer diameters, $d_p = 0.2, 0.3, 0.89$ and 1.8 mm, each with an inner-to-outer diameter ratio of 0.6. The three largest tubes were the same tubes used in the study by McKeon *et al.* (2003) (figure 2a), with the additional 0.2 mm tube made for this study having a slightly different tube support structure (figure 2b). A second 0.89 mm tube was also tested using the same support design as used for the 0.2 mm tube, and the data obtained for the 0.89 mm tubes using these two different designs were found to agree within experimental uncertainty. In the HRNBLWT four tube diameters with the McKeon *et al.* (2003) design were used, having $d_p = 0.3, 0.51, 0.89$ and 1.8 mm.

In both wind tunnels, the static pressure was measured using two static taps of diameter $d_s = 0.57$ mm connected together. The taps were positioned at the same downstream location as the tip of the Pitot tube and 6.35 mm on either side of it. The edges of the holes were inspected with an optical microscope to ensure that the taps were free of burrs and level with the plate surface.

The pressure difference between the Pitot tube and the static taps was measured using a Datametrics 1400 pressure transducer. In the KTH experiments, an additional 10 Torr MKS Baratron transducer was used in parallel as a check on the primary transducer. In the HRNBLWT, an Omega PX653-0.05BD transducer was used to verify

the low pressure sensitivity of the Datametrix transducer. In all cases, the pressures measured by the transducers were found to agree to within experimental scatter. All results presented here will be from the Datametrix transducer, which was calibrated by a professional calibration service in the period between the HRNBLWT and KTH experiments, and also checked frequently against a micromanometer to verify the stability of the transducer over time and across a range of temperatures.

Flow temperature and atmospheric pressure were monitored using the HRNBLWT and KTH transducers over the course of each profile measurement.

The Pitot tube was traversed throughout the boundary layer with measurement positions spaced logarithmically close to the wall and equidistantly in the outer part of the boundary layer. Traversing was performed using a lead screw traverse driven by a stepper motor and equipped with a linear encoder. In the HRNBLWT the traversing apparatus was a traversing sting of NACA0012 cross-section with chord length of 69.3 mm to minimize aerodynamic interference. The system is identical to that used by Hutchins *et al.* (2011). The sting was mounted to a linear rail actuated by a ball screw and stepper motor arrangement. On the basis of the steps-per-revolution of the motor and the pitch of the ball screw, the computer-controlled sting could be traversed vertically with a minimum step size of 8 μm . A Renishaw RG58C linear encoder provides a measurement of all incremental traverse movements with a resolution of 0.1 μm and accuracy of 3 $\mu\text{m m}^{-1}$. In Stockholm a smaller traversing apparatus, built around a Velmex A1509K1-S1.5 lead screw driven by a Lin Engineering micro-stepping stepper motor and controller, was used to position the probe with a minimum step size of 20 nm. Actual probe position was determined using an AcuRite SENC 50 linear encoder, with a 0.5 μm resolution and accuracy of 5 $\mu\text{m m}^{-1}$. All traverses were initiated with the Pitot tube in contact with the wall. In the KTH experiments, backlash introduced some uncertainty in determining the location of the first measurement point, so for the Melbourne experiments a Canon EOS 40D SLR camera with a 200 mm macro lens was synchronized with the traverse to provide images which were used to visually verify the point where the tube first lifted away from the wall.

Data acquisition and traverse control was provided by a 16-bit USB data acquisition system (National Instruments USB-6212). Voltages were digitized at a rate of 1 kHz with sample times adjusted from 20 s up to 2 min, depending on the flow velocity and proximity to the wall. After moving the Pitot tube, up to 20 s was allowed before acquiring data to minimize transients. Averaging and settling times were determined using preliminary measurements with the smallest Pitot tube used in each facility, based on convergence and response of the measured mean velocity.

3.3. Hot-wire measurement instrumentation and procedures

As part of this experimental campaign, measurements were also conducted using hot-wire anemometry by researchers from the University of Melbourne and KTH. The results from these experiments allow direct comparison of the results measured by both techniques at the same flow conditions and the experimental procedures used by each group are described below.

3.3.1. Melbourne University instrumentation

Measurements made by the Melbourne group were conducted with two hot-wire probes mounted side by side with their stubbed sensing elements 220 mm upstream of the leading edge of the same traversing sting used for the Pitot measurements in the HRNBLWT. One hot-wire probe had a sensing element of either 1.5 or 2.5 μm

diameter (depending on the Reynolds number) and the other probe a diameter of $5\text{ }\mu\text{m}$. Both active parts of the sensors had a length-to-diameter ratio of 200. This arrangement was found to be useful for long duration experiments where smaller wires can suffer from calibration drift, whereas larger wires have been found to be much more stable. In this way, the $5\text{ }\mu\text{m}$ probe provides a reference mean velocity profile that can be used to correct the smaller wire data if necessary (see Hutchins *et al.* 2011). For smaller wires, a custom-built constant temperature anemometer circuit (MUCTA) was used, while for the larger wires an AA Labs (AN-1003) anemometer was employed. In this paper the mean-flow hot-wire data presented are results from the larger ($5\text{ }\mu\text{m}$) sensor.

3.3.2. KTH instrumentation

The measurements by the KTH group were performed by means of a custom-built single-wire, boundary-layer-type probe. The prongs consisted of 0.5 mm diameter steel wires that were etched to give a conical tip with a diameter of around $30\text{ }\mu\text{m}$. The hot-wire itself was a stubless Platinum wire of around 0.5 mm length and nominal diameter of $2.5\text{ }\mu\text{m}$ that was soldered to the tip of the prongs facing the flat plate. A Dantec StreamLine 90N10 frame in conjunction with a 90C10 constant temperature anemometer module operated at a resistance overheat of 70% and a DISA 55M01 main frame with a 55M10 standard CTA module at an overheat of 80% were used for measurements in the MTL wind tunnel and HRNBLWT, respectively.

The hot-wires were calibrated both before and after each profile measurement in order to ensure that no drift had occurred during the measurement. The calibration was done *in situ* in the free stream against a Pitot-static tube connected to a micromanometer of type FC0510 (Furness Control Limited), from which also the ambient pressure and temperature in the tunnel were obtained.

The same traversing apparatus was used for both groups' hot-wire measurements. For the measurements in the MTL tunnel, the traversing system described in detail in Österlund (1999) was employed. It consists of a servo motor and an optical encoder with a relative accuracy of $1\text{ }\mu\text{m}$. For the measurements in the HRNBLWT the same system was used as for the Pitot tube measurements.

3.3.3. Hot-wire measurement procedures

The hot-wire measurements were performed and post-processed in a consistent way for all measurement runs by both groups. The calibration function was a third-order polynomial that was fitted to the calibration data pairs (including the voltage at zero velocity). The preliminary wall position of the sensing element was obtained optically and was adjusted by fitting the near-wall data (up to $y^+ < 20$) to a prescribed mean velocity distribution. The sampling times exceeded by far those for the Pitot tube measurements in order to ensure converged statistics for even the higher-order moments.

3.4. Oil film interferometry

Wall shear stress in both wind tunnels was determined using oil film interferometry. The basic setup employed a 35 W Phillips SOX35 low pressure sodium lamp, an optically clear insert in the bounding wall located at the same streamwise measurement station as the hot-wire and Pitot tube experiments, and a Nikon D80 (MTL) or Nikon D200 (HRNBLWT) digital camera equipped with a 200 mm , $f/4$ macro lens. The timing of each camera was verified to within 0.1 s by imaging a stop watch. Silicone oil with viscosity of 20 cSt was used to produce the oil film in both the HRNBLWT and MTL measurements, with a second 200 cSt silicone oil used in the

MTL measurements. The oil viscosity was calibrated using a capillary viscometer immersed in a temperature-regulated bath. The same Fluke thermocouple thermometer was used to monitor surface temperature as was used for calibration temperature.

In the MTL, flow conditions during shear stress measurements were monitored using a PT100 RTD temperature probe and a reference Pitot-static tube connected to a Furness FCO510 flow meter. In the HRNBLWT, flow conditions were monitored using a PT100 RTD temperature probe and Pitot-static tube connected to a MKS Baratron 698 pressure transducer monitored by a PC-based data acquisition system.

Depending on the facility, the camera was mounted on different supports designed to accurately set the angle relative to the wall-normal direction, measured by a precision level to be $15 \pm 0.5^\circ$. For each set of measurements a calibration image of millimetre paper placed on the optically clear insert was taken and repeated images indicated that accuracy of $\pm 0.1\%$ could be achieved. A silicone oil drop was then deposited with a needle on the transparent surface and the wind tunnel started. Once steady velocity was achieved, the oil film interferometry images were recorded at constant time intervals with the interval depending on oil viscosity and wall shear stress. 3872×2592 pixel² images were acquired, corresponding to a $52\text{--}72$ pixel mm^{-1} (MTL) or 124 pixel mm^{-1} resolution. Measurements with several oil drops were performed during the same runs to verify repeatability of the measurements.

Images were processed to determine the wall shear from the time rate of change of the interferometry fringes. The fringe wavelength was estimated by spanwise averaging an image strip normal to the fringes to obtain a one-dimensional signal $s(x)$. The wavelength of the fringes was then determined by maximizing the correlation between this signal and a complex exponential by means of the condition

$$\frac{d}{dk} \left| \frac{1}{L} \int_0^L s(x) e^{(2\pi i k / L)x} dx \right| = 0, \quad (3.1)$$

where $i = \sqrt{-1}$, L is the interrogation length and k is the wavenumber, thus providing the fringe wavelength as L/k . Comparison of this approach to other techniques revealed that estimation of the wall shear in this way was less user-dependent and faster to apply than other techniques.

3.5. Experimental conditions

The experimental conditions for the Pitot tube measurements are summarized in table 1. The semi-empirical skin friction relationship

$$\frac{u_\tau}{U_e} = \sqrt{\frac{C_f}{2}} = \left(\frac{1}{0.38} \ln Re_{\delta^*} + 3 \right)^{-1}, \quad (3.2)$$

determined from oil-film wall shear measurements in the KTH, Melbourne and IIT wind tunnels, was used to estimate the friction velocity, u_τ . Here U_e is the free-stream velocity, C_f is the friction coefficient, and $Re_{\delta^*} = U_e \delta^* / \nu$ is the Reynolds number based on displacement thickness δ^* .

3.6. Uncertainty estimates

Experimental uncertainties were estimated taking into account the accuracy of all parts of the experiment, and they are shown in table 2. Details of the uncertainty calculations are given in the Appendix. To provide a visual reference regarding the magnitude of the uncertainty, a single example mean velocity profile is shown in

Tunnel	Re_θ	Re_{δ^*}	U_e (m s ⁻¹)	x (m)	u_τ (m s ⁻¹)	ν/u_τ (mm)	δ (mm)	δ^+	d_p (mm)	d^+
HRNBLWT	11 400	15 100	12.6	8	0.44	0.034	119	3500	0.3, 0.51, 0.89, 1.8	9-53
HRNBLWT	16 100	21 300	12.2	13	0.42	0.036	179	5000	0.3, 0.51, 0.89, 1.8	8-50
HRNBLWT	21 400	27 700	10.7	21	0.36	0.042	271	6450	0.3, 0.51, 0.89, 1.8	7-43
HRNBLWT	44 200	56 300	24.9	21	0.78	0.019	260	13 700	0.3, 0.89	16-95
HRNBLWT	66 900	84 600	40.2	21	1.22	0.012	251	20 900	0.3, 0.89	25-150
MTL	11 200	15 000	20.0	5.5	0.70	0.022	76	3500	0.2, 0.3, 0.89, 1.8	9-82
MTL	16 100	21 300	29.9	5.5	1.02	0.015	75	5000	0.2, 0.3, 0.89, 1.8	13-120
MTL	20 500	27 300	39.8	5.5	1.33	0.012	74	6400	0.2, 0.3, 0.89, 1.8	17-150

TABLE 1. Experimental conditions.

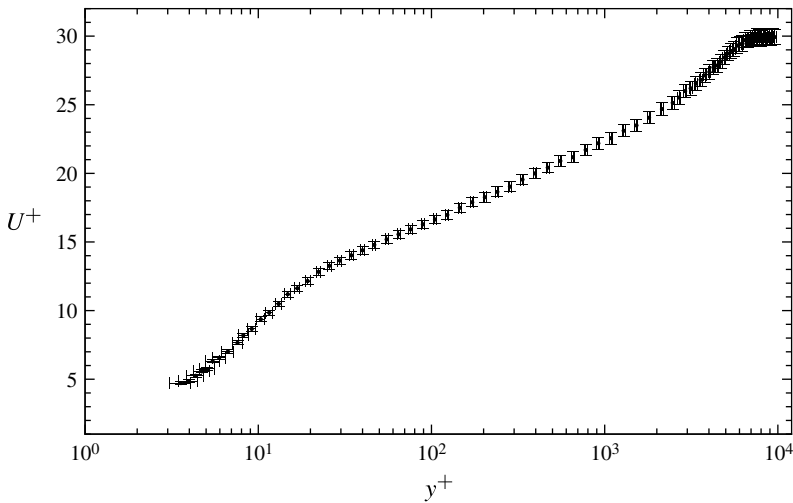


FIGURE 3. Error bars illustrating estimated error in U^+ and y^+ for 0.3 mm Pitot tube mean velocity profile from HRNBLWT at $Re_\theta = 21\,400$.

	Quantity	Notation	Uncertainty \pm
(i)	Dynamic pressure	Δp	0.4 %
(ii)	Temperature	T	0.2 %
(iii)	Atmospheric pressure	p_{atm}	0.1 %
(iv)	Air density	ρ	0.2 %
(v)	Air dynamic viscosity	μ	0.2 %
(vi)	Skin friction coefficient	c_f	3.8 %
(vii)	Viscous length scale	ℓ_*	1.9 %
(viii)	Velocity (Pitot tube)	U	0.3 %
(ix)	Inner-scaled velocity	U^+	1.9 %
(x)	Wall location	y_0	20 μm
(xi)	Relative wall position (Melbourne)	Δy	1.0 μm
(xii)	Relative wall position (KTH)	Δy	0.5 μm
(xiii)	Momentum thickness Reynolds number	Re_θ	0.9 %
(xiv)	Displacement thickness Reynolds number	Re_{δ^*}	0.7 %
(xv)	Velocity (hot-wire)	U	1.0 %

TABLE 2. Uncertainty estimates for various quantities.

figure 3 with corresponding error bars. Ensuing figures will be shown without the error bars to maintain clarity of the figures.

4. Assessment of Pitot tube corrections

All measured pressures were calculated from the mean Pitot tube pressure data and corrected for viscous effects using (2.1). However, corrections for finite static tap size were found to be negligible ($d_s^+ < 50$ for all cases), the nonlinear effects of spatial averaging are assumed small and vibration effects are not considered. In what follows,

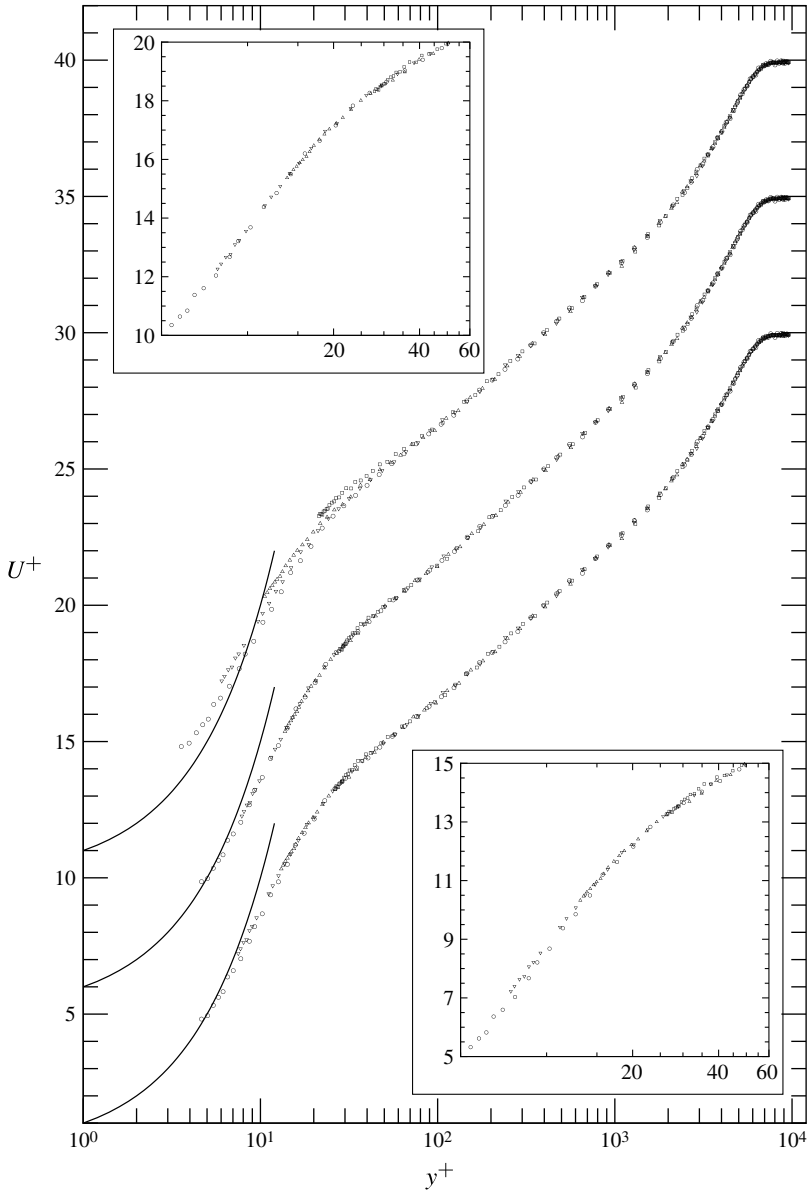


FIGURE 4. Boundary layer profiles at $Re_\theta = 21\,400$ measured in HRNBLWT using a range of Pitot tube diameters. Uncorrected profiles are shown shifted vertically by 10; profiles corrected using MacMillan corrections are shifted vertically by 5 with the bottom profiles corrected using the McKeon *et al.* corrections. The upper inset shows magnification of profiles corrected using MacMillan procedures near the wall; the lower inset shows the profiles corrected following the McKeon *et al.* procedures. Tube diameters: \circ , 0.30 mm; ∇ , 0.51 mm; \triangle , 0.89 mm; \square , 1.80 mm. Solid lines indicate $U^+ = y^+$.

we will assess the additional velocity shear and near-wall corrections, and investigate the nature of the turbulence correction.

4.1. Velocity shear correction

The results obtained using Pitot tubes with four different diameters at $Re_\theta = 21\,400$ are given in figure 4, which shows: (i) results corrected only using the viscous correction; (ii) results corrected using the viscous correction as well as the shear and near-wall corrections advocated by MacMillan; and (iii) results corrected using the viscous correction as well as McKeon *et al.* shear and near-wall corrections. Here α was determined using the velocity gradient calculated from the uncorrected velocity using a second-order accurate finite difference scheme for unequal grid spacing (Hoffman & Chiang 2000). Iterative schemes for determining α using the velocity gradient determined from a previous iteration's corrected velocity were also attempted, but found to produce no noticeable difference in the corrected profiles when compared to those corrected with α determined from velocity gradients estimated using uncorrected velocity. Note that in figure 4 the collapse of data from different tube diameters provides an indication of the capability of the corresponding corrections, with perfect collapse reflecting a correction to infinitesimal tube size. The results shown in figure 4 without shear and near-wall corrections clearly demonstrate the potential error which can be introduced if these corrections are not applied.

Far away from the wall, there appears to be little difference between the MacMillan and McKeon *et al.* corrections. To make this comparison more quantitative, we first account for the variations in y^+ measurement locations by interpolating the measured velocity data from each tube and measurement condition combination to 50 logarithmically spaced locations between $y^+ = 10$ and $y^+ = 1000$. Note that only the 10 cases with the smallest d_p could be interpolated at $y^+ = 10$. The mean, $\langle U^+ \rangle$, and two times the standard deviation, $2\langle U^+ \rangle_{std}$, of the results at each interpolated location are shown in figure 5.

Interestingly, we see a small difference in the gradient of $\langle U^+ \rangle$ evaluated using the MacMillan and the McKeon *et al.* corrections for $y^+ < 300$, indicating a greater difference between the effect of the corrections than was evident from figure 4. This difference is likely introduced by the insensitivity of the constant ϵ correction to the magnitude of the velocity shear. There is also a small difference in $2\langle U^+ \rangle_{std}$ within the range $100 < y^+ < 600$, with the results indicating a slight improvement in the collapse of the data using the corrections suggested by MacMillan. However, for $y^+ > 70$ the $2\langle U^+ \rangle_{std}$ results also show that the experimental scatter for either correction is within the estimated uncertainty in U^+ , which is illustrated by a dashed line in figure 5(b), since 95 % of data can be expected to lie within $2\langle U^+ \rangle_{std}$. Furthermore, the increase in $2\langle U^+ \rangle_{std}$ for $y^+ < 70$ can be attributed to uncertainty propagated into U^+ from the uncertainty in y^+ via the high-velocity shear near the wall, which can be estimated using $\epsilon_{y^+} \partial U^+ / \partial y^+$, where ϵ_{y^+} is the uncertainty in wall position. This additional contribution is illustrated by the dash-dotted line in figure 5(b). Therefore it appears that either shear correction provides sufficient accuracy (that is, to within experimental uncertainty).

4.2. Near-wall correction

Close inspection of the insets in figure 4 reveals that the disagreement between the different tube diameters is larger for results corrected using the McKeon *et al.* corrections than for the results corrected using the MacMillan corrections in the region where the near-wall corrections were applied ($y/d_p < 2$). McKeon *et al.*

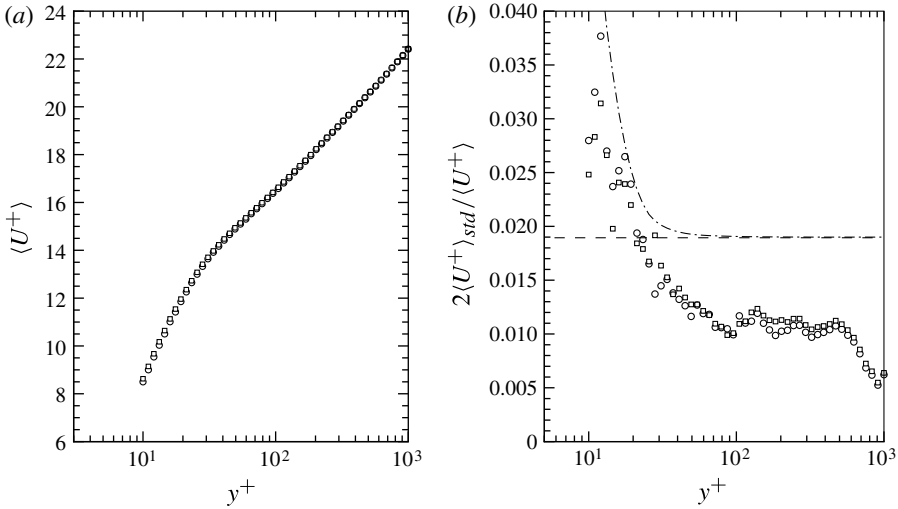


FIGURE 5. (a) Mean and (b) standard deviation of all data sets interpolated to the same y^+ locations after using MacMillan near-wall and constant ϵ corrections (\circ), and McKeon *et al.* near-wall and shear corrections (\square). The dashed line in (b) indicates estimated uncertainty in U^+ ; the dash-dotted line in (b) indicates average estimated uncertainty in U^+ when error propagated from y^+ uncertainty is included.

(2003) also observed this disagreement and suggested ignoring data measured within $1d_p$ of the wall. In the current study, we find that the source of this disagreement in the McKeon *et al.* corrections is due to the step changes amongst the three d^+ regimes in (2.6). Therefore, we suggest a modified correction for $y < 3d_p$ which does not rely on d^+ and hence *a priori* knowledge of the wall shear stress. This new correction is

$$\epsilon = 0.15 \tanh(4\sqrt{\alpha}) - \epsilon_{nw} \quad (4.1)$$

in which ϵ_{nw} accounts for the displacement of the streamlines due to near-wall blockage effects and can be found from

$$\epsilon_{nw} = \beta_1(y/d_p - 3) + \beta_2(y/d_p - 3)[0.15 \tanh(4\sqrt{\alpha})], \quad (4.2)$$

where $\beta_1 = 0.174$ and $\beta_2 = -1.25$. The new near-wall correction is compared to the original McKeon *et al.* near-wall correction in figure 6, and the resulting collapse can be seen to be comparable to the collapse resulting from application of the MacMillan correction.

In general, we recommend the correction embodied in (4.1) for the near-wall region for all future use of Pitot tubes when $d^+ < 150$ in wall-bounded flows, in that it accounts for the possibility of uniform flow (in contrast to MacMillan's correction procedure), it improves the McKeon *et al.* formulation, and will admit measurements for $y < d_p$ (in contrast to the McKeon *et al.* correction procedure).

In the absence of turbulence effects, a complete Pitot tube correction process is therefore as follows: (i) apply the viscous correction for static taps if necessary (see McKeon & Smits 2002, for example); (ii) apply the viscous correction of (2.1) when $Re_d < 100$; (iii) correct the results for $y/d_p > 3$ for shear using the McKeon *et al.* shear correction using (2.3); and (iv) apply the modified McKeon *et al.* near-wall correction for $y/d_p < 3$ using (4.1).

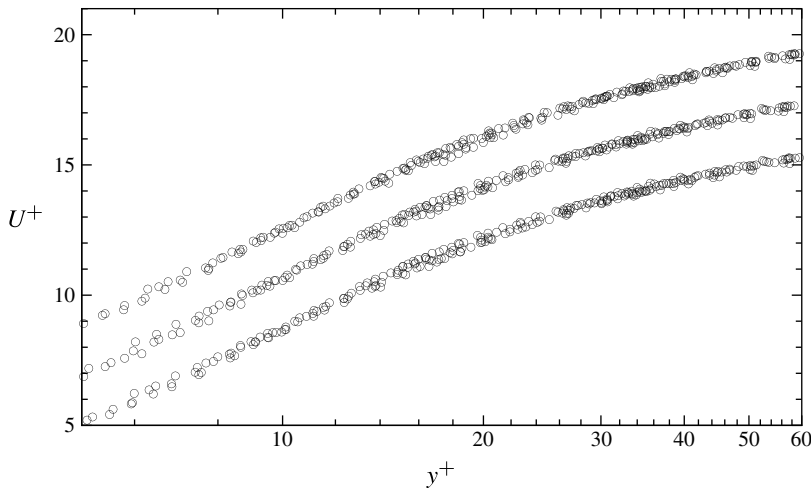


FIGURE 6. Comparison of viscous, shear and near-wall effect corrected data from the Melbourne experiments using: (bottom) the proposed near-wall correction of (4.1) and McKeon *et al.* shear correction; (middle) the original McKeon *et al.* near-wall and shear correction; and (top) the MacMillan near-wall and constant ϵ correction. Original McKeon *et al.* corrected data shifted vertically by 2 and MacMillan corrected data shifted vertically by 4.

4.3. Turbulence correction

The average total pressure measured by a Pitot tube is nonlinearly related to velocity, and so we expect there to be a contribution from the velocity fluctuations, introduced during averaging. This can be shown analytically (Goldstein 1938) by integrating the equation of motion of a fluid element moving along a streamline (Euler's equation). For incompressible flow, we obtain

$$\frac{p}{\rho} = -\frac{1}{2}u_s^2 - \int \frac{\partial u_s}{\partial t} ds + c(t), \quad (4.3)$$

where s is the coordinate along the streamline, u_s is the velocity in the s -direction, t is time, p is the pressure, and $c(t)$ is a time-varying constant of integration. For turbulent shear flows u_s can vary in magnitude and direction, so we can rewrite u_s using Cartesian velocity components u, v, w , where $u_s^2 = u^2 + v^2 + w^2$. In addition, these velocity components may be decomposed into mean and fluctuating contributions, U and u' , V and v' , W and w' respectively. Applying the same decomposition to pressure such that $p = P + p'$, substituting into (4.3) and time-averaging the result gives

$$\frac{P}{\rho} + \frac{1}{2}(U^2 + V^2 + W^2 + \overline{u'^2} + \overline{v'^2} + \overline{w'^2}) = \text{constant}, \quad (4.4)$$

where the constant of integration is commonly referred to as the total pressure. Equation (4.4) differs from the classical Bernoulli equation only by the turbulence intensity terms, $\overline{u'^2}$, $\overline{v'^2}$ and $\overline{w'^2}$. With the Pitot tube aligned with U such that $V = W = 0$ and introducing ΔP as the difference between the total and static pressure, (4.4) can be used to determine the following relationship:

$$\Delta P = \frac{1}{2}\rho(U^2 + \overline{u'^2} + \overline{v'^2} + \overline{w'^2}). \quad (4.5)$$

In fact, the mean flow orientation impinging on the probe face will not be exactly parallel to the probe, due to the combined effects of velocity shear and near-wall blockage. However, the effect of the non-zero transverse components of the mean velocity at the probe face should be negligible following application of shear and near-wall corrections. Since the essence of these corrections is to adjust measurement position and velocity to remove the influence of the probe presence from the mean flow, they artificially move the measurement position to a location where the mean flow is parallel to the wall.

Since a Pitot tube (combined with a static pressure reference) measures ΔP , the measured velocity U_m overestimates the true velocity U according to

$$U_m = \sqrt{U^2 + \overline{u'^2} + \overline{v'^2} + \overline{w'^2}}. \quad (4.6)$$

This result applies to any Pitot tube, regardless of diameter (as long as spatial filtering effects are small).

As is commonly done in Pitot turbulence corrections, an estimate of the true velocity can be easily determined from the measured velocity using (4.5), as given by

$$U^+ = \frac{U}{u_\tau} = \sqrt{\left(\frac{U_m}{u_\tau}\right)^2 - \frac{\overline{u'^2}}{u_\tau^2} - \frac{\overline{v'^2}}{u_\tau^2} - \frac{\overline{w'^2}}{u_\tau^2}}. \quad (4.7)$$

Equation (4.7) assumes that the Pitot tube is always aligned with the flow streamline and neglects fluctuations in the orientation of the streamlines impinging on the Pitot tube face. This observation can be accommodated through the introduction of a factor, as is done in (2.8) for example, to account for effects of anisotropy, scale and structure of the turbulence. We now evaluate the need for additional modifications to (4.7) using a new approach.

We first note that a misalignment in direction between the streamline and tube in the mean will cause a decrease in measured total pressure proportional to the angle θ between the two directions (Chue 1975). We will therefore assume a quasi-steady behaviour such that

$$U_m^2 = (\overline{f(\theta)} + 1)(U^2 + \overline{u'^2} + \overline{v'^2} + \overline{w'^2}), \quad (4.8)$$

where $\overline{f(\theta)}$ is the average value of a coefficient reflecting the decrease in measured velocity relative to the true velocity due to the instantaneous value of θ , as given by Chue (1975), which we have simplified to the polynomial representation given by

$$f(\theta) = \frac{U_m^2 - U^2}{U^2} = -0.56\theta^2 - 0.88\theta^4 + 0.85\theta^6, \quad (4.9)$$

where θ is in radians.

To determine the average value of $f(\theta)$, at a specific wall-normal position, we will use a probability density function (p.d.f.) of the flow angle. This p.d.f. does not have to be determined directly, but can be estimated through the p.d.f. of the velocity fluctuations $g(u', v', w')$ at each wall-normal position, which we will approximate using a trivariate normal p.d.f.

$$g(u', v', w') = \frac{1}{2\pi^{3/2} |\Sigma|^{1/2}} \exp \left[-\frac{1}{2} ([u', v', w'] \Sigma^{-1} [u', v', w']^T) \right], \quad (4.10)$$

where for boundary layers

$$\Sigma = \begin{pmatrix} \overline{u'^2} & \overline{u'v'} & 0 \\ \overline{u'v'} & \overline{v'^2} & 0 \\ 0 & 0 & \overline{w'^2} \end{pmatrix}. \quad (4.11)$$

We can then estimate $\overline{f(\theta)}$ using

$$\overline{f(\theta)} = \int_{-\infty}^{+\infty} \int_{-\infty}^{+\infty} \int_{-\infty}^{+\infty} f(\theta) g(u', v', w') du' dv' dw', \quad (4.12)$$

where

$$\theta = \tan^{-1} \left(\frac{\sqrt{v'^2 + w'^2}}{(U + u')} \right). \quad (4.13)$$

The magnitude of the bias expected from the nonlinear averaging of the velocity fluctuations can be estimated by examining profiles of the quantity $q_1 = (U^2 + \overline{u'^2} + \overline{v'^2} + \overline{w'^2})^{1/2} / U - 1$, as shown in figure 7(a). To estimate this quantity, we use the Schlatter & Örlü (2010) direct numerical simulation (DNS) data and DeGraaff & Eaton (2000) laser Doppler velocimetry (LDV) data, along with the approximation $\overline{w'^2} \approx \overline{v'^2}$ applied to the LDV data. The values shown in figure 7(a) demonstrate that the greatest bias due to nonlinear averaging of the velocity fluctuations occurs for $y^+ < 30$, approaching 12 % of U at $y^+ = 1$ for the Reynolds numbers shown. At $y^+ = 30$, the expected bias exhibits only weak Reynolds number dependence and is approximately 2 % of U . For $y^+ > 30$, the bias decreases monotonically to zero with increasing wall-normal distance.

These results can be compared to profiles of $q_2 = (U^2 + \overline{u'^2})^{1/2} / U - 1$ from the same data sets, shown in figure 7(b), which illustrates the expected bias introduced solely due to effect of nonlinear averaging of the velocity fluctuations. As could be expected, the major part of the error is introduced by this effect, although, as seen by examining the difference $q_1 - q_2$ shown in figure 7(c), neglecting the transverse stresses could result in under-correction by as much as 0.5 % for $y^+ > 30$. Although this is not a large contribution to the overall expected nonlinear averaging bias, we see that neglecting the transverse stresses can result in a 2.5 % under-correction for $y^+ < 30$.

It would appear, therefore, that an accurate turbulence correction needs to include the transverse as well as the streamwise Reynolds stresses. However, when the magnitude of the bias expected from the instantaneous tube misalignment, $(\overline{f(\theta)} + 1)^{1/2} - 1$, shown in figure 7(d) is compared to figure 7(c), we see that the misalignment contribution counters the effect of neglecting the transverse Reynolds stresses (note that the vertical axis of figure 7d has been inverted for better comparison to figure 7a–c). Thus, the increase in measured velocity caused by fluctuations in the magnitude of the velocity are counter-balanced by a corresponding decrease in measured velocity due to fluctuations in the orientation of the velocity vector at the tube face. This is not wholly unexpected, given that the transverse velocity fluctuations are directly correlated to the direction of the streamline with respect to the tube axis. Thus

$$U_m^2 = (\overline{f(\theta)} + 1)(U^2 + \overline{u'^2} + \overline{v'^2} + \overline{w'^2}) \approx (U^2 + \overline{u'^2}), \quad (4.14)$$

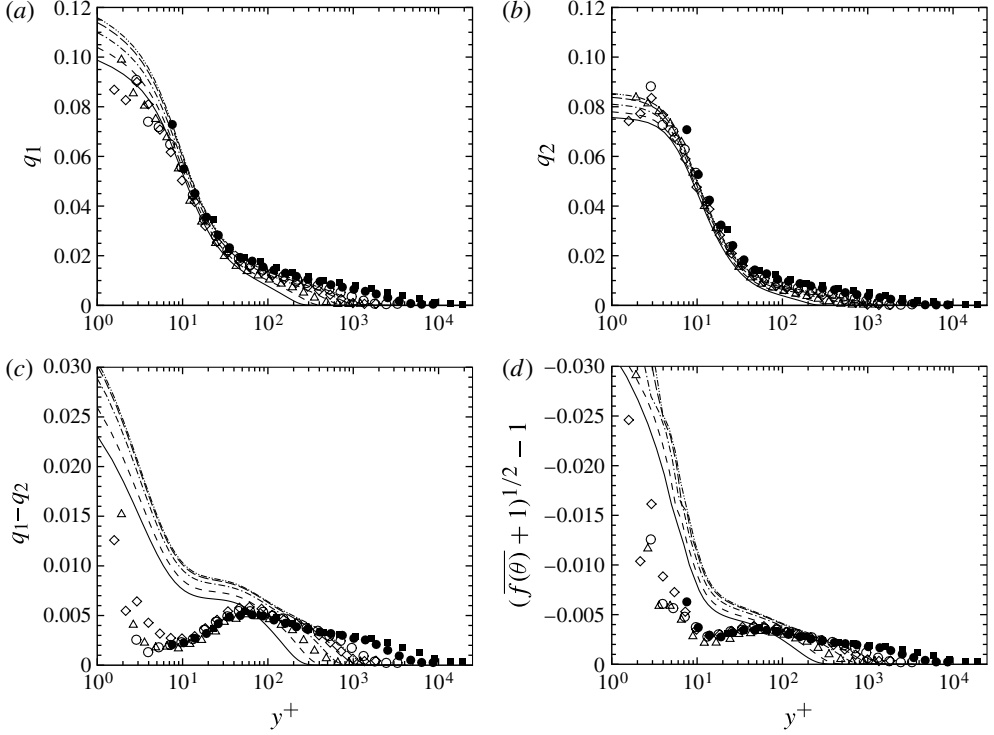


FIGURE 7. Expected bias introduced in Pitot measurements due to: (a) nonlinear averaging of instantaneous misalignment between the streamline and Pitot; (b) nonlinear averaging neglecting transverse stresses $\overline{v'^2}$ and $\overline{w'^2}$; (c) only the transverse stresses $\overline{v'^2}$ and $\overline{w'^2}$; and (d) instantaneous fluctuations in the velocity vector. Quantities estimated using the DNS of Schlatter & Örlü (2010): —, $Re_\theta = 670$; - - -, $Re_\theta = 1000$; - · - ·, $Re_\theta = 2000$; - - -, $Re_\theta = 3030$; - · · - ·, $Re_\theta = 4060$. Also shown is the same quantity calculated from LDV measurements of DeGraaff & Eaton (2000): \triangle , $Re_\theta = 1490$; \diamond , $Re_\theta = 2900$; \circ , $Re_\theta = 5200$; \bullet , $Re_\theta = 13000$; \blacksquare , $Re_\theta = 31000$.

and the effect of turbulence on the Pitot tube velocity can be corrected simply via

$$U \approx \sqrt{U_m^2 - u'^2} \quad (4.15)$$

with an expected magnitude of the correction on U being less than 1.5% for $y^+ > 30$ and $Re_\theta < 31000$. It should be noted that, although small, the wall-normal dependence of the bias introduced by turbulence effects could affect the estimate of the von Kármán constant. This will be examined in greater detail in a companion paper.

4.4. Revised wall-proximity correction for use in turbulence correction

As discussed in §2, flow blockage introduced by the tube approaching the wall results in a deflection of the streamlines away from the wall. Near-wall corrections, such as those proposed by McKeon *et al.* (2003), are typically designed to correct the data near the wall onto a formulation for the velocity profile (for example, $U^+ = y^+$ in the viscous region, or the log-law in the overlap region). Such schemes therefore correct for shear, wall-proximity and turbulence effects. Thus, such corrections are inappropriate when a separate turbulence correction is employed.

It is necessary, therefore, to determine a new correction which will correct only for wall-proximity effects. It was found that a simple modification to the MacMillan wall-proximity correction, given by

$$\frac{\Delta U}{U} = (20e^{-0.1d^+} + 1)0.015e^{-2.5(y/d_p - 0.5)} \quad (4.16)$$

within the range $y < 2d_p$, effectively corrects the data for $7 < d^+ < 160$. This wall-proximity correction is to be applied after the shear correction is applied. Note that for $d^+ > 50$ the correction is effectively equivalent to that originally proposed by MacMillan, with only a slight change to the exponent to account for the y/d_p dependence observed in the current data set. It should also be noted that (4.16) re-introduces dependence on d^+ into the near-wall correction, and thus requires some estimate of the wall shear stress.

In the presence of turbulence effects, a complete Pitot tube correction process is therefore as follows: (i) apply the viscous correction for static taps if necessary (see McKeon & Smits 2002, for example); (ii) apply the viscous correction (equation (2.1)) when $Re_d < 100$; (iii) apply the shear correction proposed by McKeon *et al.* (2003) ((2.2) and (2.3)) for all wall-normal positions; (iv) apply the near-wall correction proposed in (4.16) for $y < 2d_p$; and (v) apply the turbulence correction of (4.15). Note that, since (4.15) requires *a priori* knowledge of the profile of streamwise Reynolds stress, application of a turbulence correction could be impractical in generalized wall-bounded flows. Even when a turbulence intensity formulation is available, often the scaling and measurement accuracy of these values remains an open question; see Mochizuki & Nieuwstadt (1996), Metzger *et al.* (2001), Morrison *et al.* (2004) and Hutchins *et al.* (2009), for example.

5. Comparison to hot-wire data

The turbulence correction given by (4.15) was proposed under the assumption that no filtering of the velocity fluctuations occurs before averaging. Such filtering might occur due to spatial averaging of velocity fluctuations across the face of the tube, or through the response of the transducer and tubing system. In addition, modern measurement systems (such as fast-response multi-hole probes) allow the measurement of pressure time series, making it possible to average after conversion to velocity, introducing effects of temporal filtering caused by the dynamic response of the measurement system. Hence, the validity and magnitude of the turbulence correction as proposed needs to be assessed.

As part of the ICET measurement campaign, a series of hot-wire measurements were performed by research groups from Melbourne and KTH at identical conditions to the Pitot measurements for $Re_\theta = 11\,000$, $16\,000$ and $21\,000$. These hot-wire results offer a unique opportunity to compare results from these two measurement techniques as well as assess the effectiveness of the turbulence correction.

Figure 8 makes this comparison for the 0.3 mm diameter Pitot results. In general, the hot-wire and Pitot results exhibit exceptional agreement, being within $0.2u_\tau$ for $y^+ > 300$, or $\pm 1\%$ of U^+ and within the expected uncertainty for the Pitot tube measurements. For $20 < y^+ < 300$ the Pitot tubes clearly measure higher values of U relative to that of the hot-wire probe, with differences of $0.5u_\tau$ (up to 4% in U). This trend is consistent with the bias expected from turbulence effects, in that the two measurement techniques agree in the wake region where turbulence intensity is low

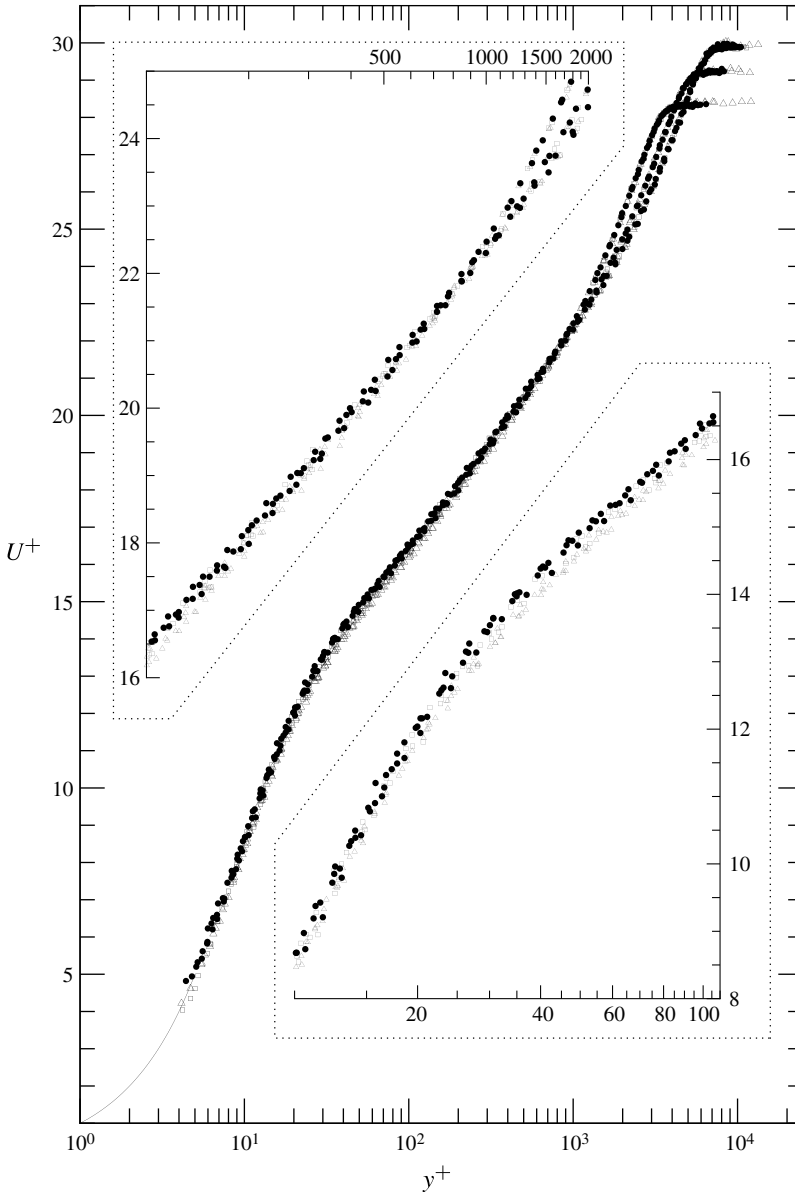


FIGURE 8. Comparison of 0.3 mm Pitot results corrected using the viscous, shear and near-wall corrections of (2.1), (2.3) and (4.1) to hot-wire measurements at $Re_\theta = 11\,000$, $Re_\theta = 16\,000$ and $Re_\theta = 21\,000$ from both MTL and HRNBLWT facilities: \bullet , Pitot; \square , KTH group hot-wire results; \triangle , Melbourne group hot-wire results.

and in the near-wall region where the wall-proximity correction has corrected the Pitot tube for turbulence effects.

As shown in figure 9, the turbulence correction brings the Pitot tube measurements into closer agreement with the hot-wire measurements, particularly within the range $20 < y^+ < 300$, although it was found to slightly over-correct relative to the hot-

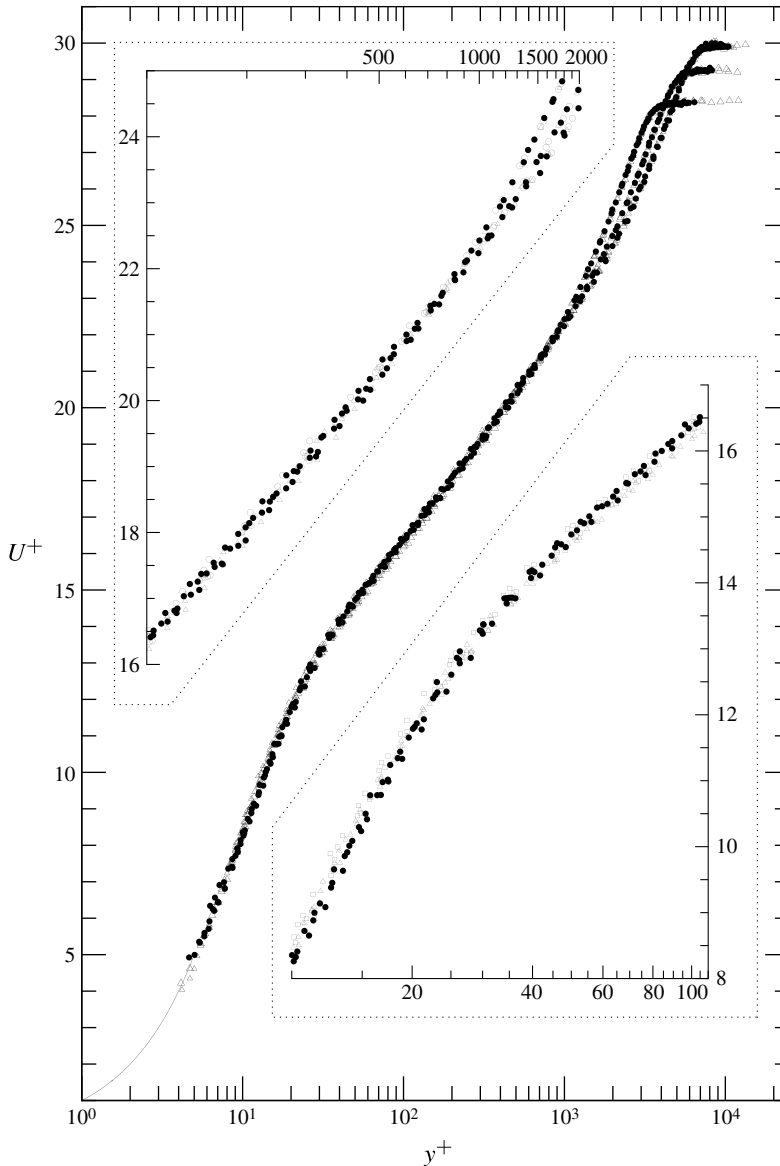


FIGURE 9. Comparison of 0.3 mm Pitot results corrected using the viscous, shear, near-wall and turbulence corrections of (2.1), (2.3), (4.16) and (4.15) to hot-wire measurements at $Re_\theta = 11\,000$, $Re_\theta = 16\,000$ and $Re_\theta = 21\,000$ from both MTL and HRNBLWT facilities: ●, Pitot; □, KTH group hot-wire results; △, Melbourne group hot-wire results.

wire for $10 < y^+ < 20$, perhaps reflecting errors introduced through a combination of neglecting the transverse Reynolds stresses and uncertainty in the turbulence intensity formulation. However, the results, in general, support the hypothesis that a turbulence correction is necessary for Pitot tubes near the wall. Note that for the Pitot profiles without the turbulence correction, there is a prominent ‘hump’ in this region (figure 8) which is largely removed by application of the turbulence correction (figure 9).

The trend demonstrated between figures 8 and 9 supports the need for a turbulence correction for Pitot tube measurements of the turbulent boundary layer, but the magnitude and applicable range of wall-normal distances requiring correction cannot be quantitatively determined from the present results. First, for $y^+ > 300$, the Pitot results, both with and without turbulence correction applied, agree with the hot-wire results within $\pm 1\%$, and therefore any differences lie within experimental uncertainty; also implying that within this y^+ range the correction itself lies within the bounds of experimental uncertainty. Second, the hot-wire results themselves are subject to experimental uncertainty, and therefore it would be remiss to assume that they precisely represent the true mean velocity profile.

6. Conclusions

Zero-pressure-gradient flat plate boundary layer velocity profiles were measured in two different wind tunnels at relatively high Reynolds numbers. It was shown that accurate profiles can be acquired with Pitot tubes, and that the measurements are insensitive to tube diameter when either the constant ϵ or McKeon *et al.* shear correction is used. The constant ϵ correction has the advantage of being easy to implement, but the McKeon *et al.* approach, with its shear-dependent displacement correction, will prevent over-correction in regions with low shear. A modified near-wall adjustment to the McKeon *et al.* correction has been proposed and shown to provide noticeable improvement over the original form, although the final results are very similar to those obtained using the MacMillan near-wall correction and have not been validated above $d^+ = 150$. However, the corrections presented here are expected to be generally applicable to both shear flows and wall-bounded flows.

The bias error introduced by nonlinear averaging of the turbulent velocity fluctuations was also investigated. It was found that, although fluctuations in all three components of velocity should be considered, the Pitot tube's angular sensitivity provides some compensation for the transverse fluctuations, so that a correction based on only the velocity fluctuations in the streamwise direction was found to be sufficient. Correcting for the turbulent fluctuations in addition to corrections for velocity shear effects required the implementation of a new near-wall correction.

The Pitot results corrected for viscous, shear and near-wall effects with and without the turbulence correction were compared to hot-wire measurements to evaluate the effectiveness of the turbulence correction. The magnitude of the expected correction was found to be relatively small, within 2% for $y^+ > 30$, and with or without the turbulence correction the Pitot tube and hot-wire results agreed to within 1% for the majority of the boundary layer (in our experiments, for $y^+ > 300$). Improved agreement was only clearly demonstrated for $y^+ < 200$. Within this region the streamwise turbulence-intensity correction can be of comparable magnitude to that of the shear correction, and is found to bring the hot-wire and Pitot results in closer agreement when applied to the data along with the other corrections discussed and refined here. The overall trend suggested that the correction may also be effective further from the wall as well.

Given that, for boundary layers, the inner-scaled turbulence intensity is expected to increase with Reynolds number, while the inner-scaled mean does not, the potential bias introduced into Pitot profiles by the turbulence may increase with Reynolds number. This is particularly relevant given that the magnitude of this bias is expected to vary with wall position, thereby potentially altering the slope of the logarithmic region. Considering the limited range of the Reynolds numbers considered here,

further studies at higher Reynolds numbers would be needed to confirm the need for turbulence correction at very high Reynolds numbers. It is also noted that the assessment presented here is limited to the zero-pressure-gradient boundary layer, and although potentially applicable to other simple turbulent wall-bounded flows, the observations cannot be extended to more complex flows, such as those found in strong adverse pressure gradients or three-dimensional boundary layers. In such flows, the effects of other Reynolds stresses and changes to the integral scales of turbulence could introduce additional effects not considered here.

We make no recommendation as to whether to use hot-wires or Pitot tubes for measurement of mean flow, as that determination will depend on the details of the experiment and the preferences of the experimentalist. The present results confirm that, when properly corrected, Pitot tubes can measure mean velocity with an accuracy comparable to that of hot-wire probes and there are advantages to either approach. Although the hot-wire probe requires no correction for turbulence effects, obtaining accurate mean flow measurements is still quite challenging. For example, disagreement between different hot-wire probe profiles measured at the same flow conditions contributed significantly to our inability to conclusively evaluate the turbulence correction for the Pitot tubes. In this regard, the simplicity of the Pitot tube and its application can make it preferable to hot-wires.

It is therefore suggested that Pitot tube measurements performed in turbulent boundary layers be corrected using a viscous correction when $Re_d < 100$ using (2.1), followed by a McKeon *et al.* shear correction using (2.3), followed by application of the near-wall blockage correction of (4.16) for $y/d_p < 2$, followed by the turbulence correction of (4.15) using a suitable estimate for the streamwise turbulence intensity. Should an estimate of the turbulence intensity be unavailable, mean velocity measurements within 5% of the true velocity for the inner layer and 1% of the true velocity for the outer layer can be obtained using a static tap and a viscous correction, the McKeon *et al.* shear correction using (2.3), and the modified McKeon *et al.* near-wall correction for $y/d_p < 3$ using (4.1). The constant ϵ shear and near-wall correction of MacMillan (1957) can also be used, as they were found to provide virtually identical results and are easier to apply, but they also unnecessarily bias the tube position in regions of low shear.

The relative magnitude of each of the correction procedures discussed here is summarized in figure 10, which compares a single profile corrected only for viscous effects to the same results corrected further using: (i) the MacMillan shear and near-wall blockage correction; or (ii) the McKeon *et al.* shear correction with the near-wall blockage correction of (4.1); or (ii) the McKeon *et al.* shear correction, the near-wall blockage correction of (4.16) and additional turbulence correction of (4.15).

This last correction procedure was applied to all Pitot tube data acquired in the MTL and HRNBLWT experiments. For simplicity and consistency, we employed the streamwise turbulence intensity formulation of Marusic & Kunkel (2003) in (4.15). It is believed that over the Reynolds number range of the current investigation, this formulation is sufficiently accurate to apply the turbulence correction to the current data set. The resulting velocity profiles obtained from all Pitot tubes, Reynolds numbers and facilities are shown in figure 11.

In figure 11 a single case is observed to deviate from the trend displayed by the remaining data sets. This particular case is the 0.89 mm tube at $Re_\theta = 44\,200$ in the HRNBLWT. The most likely source of this discrepancy is uncertainty in the initial probe position. The error is approximately 4 viscous units, which exceeds the estimated uncertainty in initial position of approximately 1 viscous unit for this case

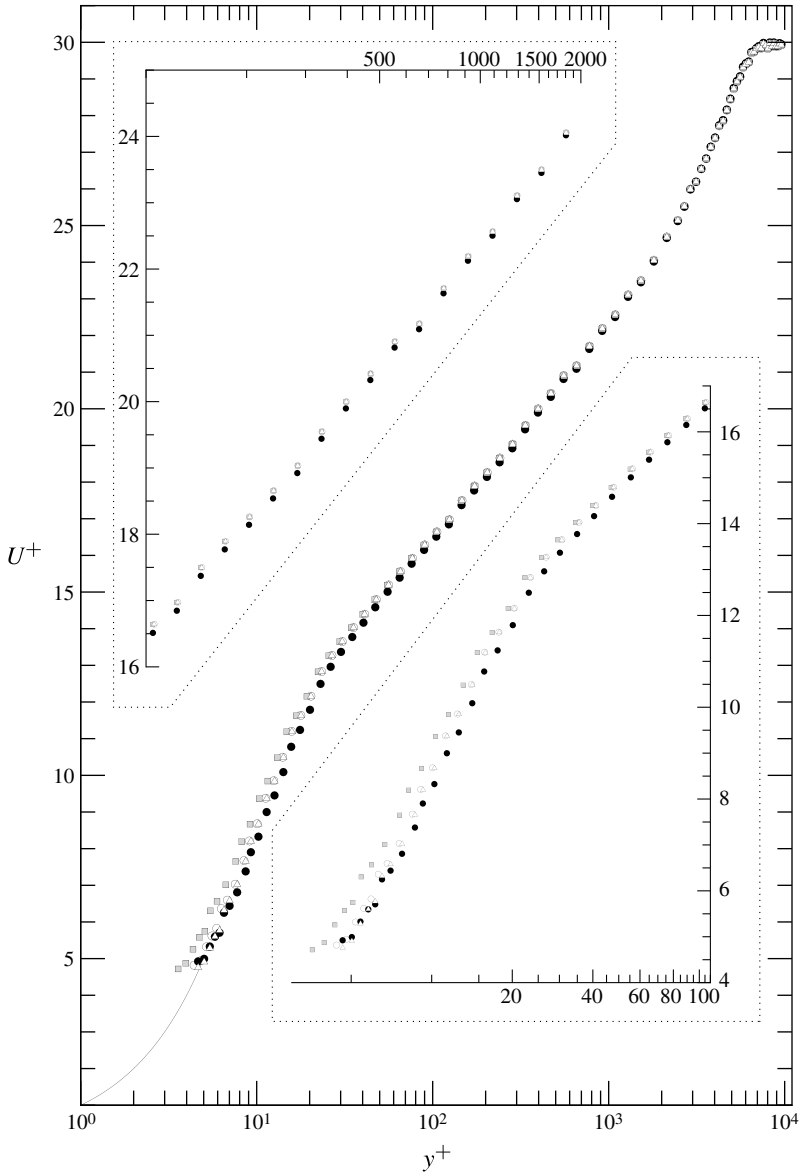


FIGURE 10. Velocity profile measured by 0.3 mm diameter tube at $Re_\theta = 21\,400$: \square , viscous correction only; \triangle , profile corrected using viscous and MacMillan shear ((2.2) with $\epsilon = 0.15$) and near-wall corrections (2.5); \circ , profile corrected using viscous and McKeon *et al.* shear correction (2.3) with near-wall correction of (4.1); \bullet , profile corrected using viscous and shear (2.3) corrections with additional turbulence and near-wall corrections of (4.7) and (4.16).

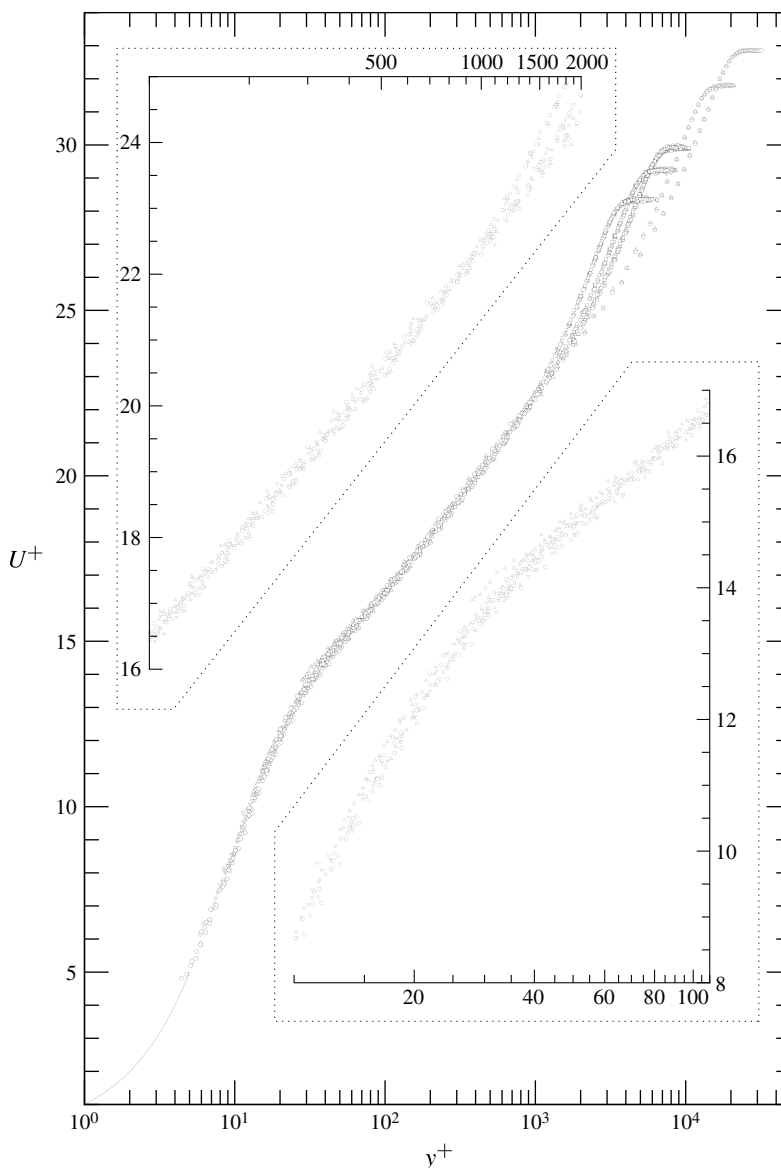


FIGURE 11. All 28 measured velocity profiles after viscous, shear, near-wall and turbulence corrections applied using (2.1), (2.3), (4.16) and (4.15). Tube diameters: \diamond , 0.2 mm; \circ , 0.3 mm; ∇ , 0.51 mm; \triangle , 0.89 mm; \square , 1.8 mm.

and represents an outlier in the initial position estimate. Given that this is the only case which displays such deviation, it represents 3.5 % of the data set and remains consistent with our 95 % confidence interval of 1 viscous unit.

Acknowledgements

This work was made possible by financial support from the Australian Research Council, the Linné FLOW centre, and ONR under Grant N00014-09-1-0263. Partial

support was also provided by the NASA Space Grant Program. The authors would also like to thank Anand Ashok, K. Chauhan, K. Dressler, G. Elsinga, S. Imayama, T. Kurian, R. Mathis, M. Matsubara, P. Monkewitz, H. Ng, E. Robert, P. Rozier, J.-D. Rüedi, A. Talamelli, Y. Tsuji and M. Vallikivi for their assistance and support throughout the course of setting up, conducting and analysing the experiments performed over the course of this measurement campaign.

Appendix. Uncertainty analysis

In this appendix the uncertainty analysis of various quantities in these experiments is given (see table 2 for the results of the analysis).

Uncertainties may be divided into bias errors and precision errors. The Pitot tube measurements are vulnerable to both types, where the wall-proximity, shear and turbulence effects can be seen as bias errors and it is the purpose of the present paper to find correction methods for these errors. Hence such effects are not taken into account in the uncertainty analysis presented here. When applicable the uncertainties are given as the value specified by the manufacturer of the given instrument, and in cases when a quantity is calculated from several measurements the method of propagation of errors is used. The uncertainty estimates given should be seen as 20:1 odds uncertainty (i.e. 95 % confidence interval).

In the following, uncertainties of the various quantities given in table 2 are discussed.

- (i) Dynamic pressure. This is the pressure difference measured between the Pitot tube and the wall pressure tap. Three possible sources contribute to the uncertainty: (a) calibration uncertainty of the pressure transducer; (b) insufficient averaging time of the transducer signal; (c) insufficient settling time after movement of the probe. The stated uncertainty of 0.4 % is from the manufacturer's specified accuracy. Both the sampling time (20 s up to 2 min, depending on flow velocity and proximity to the wall) and the settling time (20 s) after the probe has been moved are long enough, and the contribution to the uncertainty from these is small and does not add to the uncertainty given above.
- (ii) Temperature. This is the temperature of the air, and it is needed in order to determine its density and the dynamic viscosity. One should note that a probe immersed in an air flow does not measure the static temperature but probably something closer to the stagnation temperature (or rather the recovery temperature). However, to determine the density it is the static temperature that should be used in the ideal gas law. At the highest velocities here (i.e. 40 m s^{-1}) the stagnation and static temperature differ with almost 0.3 %, although this is not taken into account in the determination of the temperature. In addition, the uncertainty of the measured temperature depends on the calibration of the temperature-measuring device. The flow temperature was measured by means of the respective tunnels' transducers (PT100 at KTH, thermocouple at HRNBLWT). The readings from these were found to be within $\pm 0.1^\circ\text{C}$ compared to a reference thermometer.

Variations of the wind tunnel temperature during a measurement also adds to the uncertainty estimate. The MTL wind tunnel has good temperature control through a heat exchanger and varies with less than $\pm 0.1^\circ\text{C}$ during a measurement series. The HRNBLWT, at the time of the measurements, did not have a heat exchanger, and the temperature variation was hence higher. At

the low velocity, $U_\infty \approx 10 \text{ m s}^{-1}$, the variation is within $\pm 0.1^\circ\text{C}$ during one profile measurement, at $U_\infty \approx 25 \text{ m s}^{-1}$ the variation is within $\pm 0.25^\circ\text{C}$, but at 40 m s^{-1} the temperature increases with $\sim 2.5^\circ\text{C}$ during the measurement of one profile.

From what is discussed above it is clear that the largest temperature uncertainty appears at high velocity and may be of the order of $\pm 0.5\%$. However, this is a clear overestimate for the lower velocities, where a conservative estimate is as good as $\pm 0.2\%$.

- (iii) The atmospheric pressure was obtained by means of an absolute pressure transducer connected to the respective tunnels' transducers. For both tunnels the transducer accuracy is 0.1% of full scale reading (which is slightly above atmospheric pressure). An additional uncertainty could be the difference between the pressure measured outside the test section and the pressure inside the test section. This pressure difference is assumed to be negligible, since in the MTL tunnel there are vents at the end of the test section. Also in the HRNBLWT there may be some difference between the pressure inside the tunnel and the atmosphere, but there are vents in the upper wall to ensure a zero pressure gradient.
- (iv) The density is calculated by the ideal gas law, where the value of specific gas constant used is $R = 287 \text{ J kg}^{-1} \text{ K}^{-1}$. According to the propagation of uncertainties we get

$$\epsilon_\rho = (\epsilon_p^2 + \epsilon_T^2)^{1/2}, \quad (\text{A } 1)$$

giving a density uncertainty within $\pm 0.3\%$.

- (v) The dynamic viscosity was calculated with the Sutherland formula

$$\mu = 1.458 \times 10^{-6} \frac{T^{3/2}}{T + 110.4} \text{ kg m}^{-1} \text{ s}^{-1}. \quad (\text{A } 2)$$

The main uncertainty comes from the measured temperature ($\pm 0.2\%$) and the resulting uncertainty in μ is of similar order; $\epsilon_\mu = \pm 0.2\%$.

- (vi) The skin friction used here is based on another set of experiments, taken in conjunction with the present measurements, but will be thoroughly discussed in a separate paper. Here there are two different issues: (a) the uncertainty in the determination of τ_w for each measured oil drop; (b) the possible bias error of the different wind-tunnel setups. The data have been fitted to the logarithmic skin friction relation

$$\frac{C_f}{2} = (\kappa^{-1} \ln Re_{\delta^*} + C)^{-2}, \quad (\text{A } 3)$$

and the constants have been determined to be $\kappa = 0.38$ and $C = 3.0$. The data from the different wind tunnels where the oil film measurements have been performed (MTL, HRNBLWT and NDF) shows some consistent deviations, which should be seen as a bias error rather than a precision error. For the individual oil drops the 95 % confidence level uncertainty for a given condition in a given tunnel becomes of the order of 0.7% of τ_w ; however, for the fit of all oil-film data to the skin friction law the 95 % confidence level uncertainty becomes 3.8% for C_f , meaning that the precision error is almost negligible.

(vii) The viscous length scale is calculated as

$$\ell_* = \frac{\mu}{\rho U_\infty} \frac{2}{\sqrt{C_f}}, \quad (\text{A } 4)$$

and the uncertainty as

$$\epsilon_{\ell_*} = \sqrt{\epsilon_\mu^2 + \epsilon_\rho^2 + \epsilon_{U_\infty}^2 + 0.25\epsilon_{C_f}^2}. \quad (\text{A } 5)$$

(viii) The velocity is calculated as $U = \sqrt{2\Delta p/\rho}$ and the uncertainty is hence calculated as

$$\epsilon_U = \sqrt{0.25\epsilon_{\Delta p}^2 + 0.25\epsilon_\rho^2}, \quad (\text{A } 6)$$

which does not include bias errors from wall-proximity, shear and turbulence effects. However, there is also an effect of compressibility that for small Mach numbers can be expressed as

$$\frac{U_{\text{compr}}}{U_{\text{incompr}}} = 1 - \frac{1}{8}M^2 + O(M^4). \quad (\text{A } 7)$$

For 40 m s^{-1} this (bias) error in U amounts to 0.2% and is included in the uncertainty estimate.

(ix) Inner-scaled velocity $U^+ = U/u_\tau$. The expression for U^+ can be rewritten as

$$U^+ = \frac{U}{U_\infty} \sqrt{\frac{2}{C_f}} = \sqrt{\frac{\rho_\infty}{\rho} \frac{\Delta p}{\Delta p_\infty} \frac{2}{C_f}}. \quad (\text{A } 8)$$

The uncertainty is calculated as

$$\epsilon_{U^+} = \sqrt{0.25\epsilon_{\rho_\infty/\rho}^2 + 0.25\epsilon_{\Delta p}^2 + 0.25\epsilon_{\Delta p_\infty}^2 + 0.25\epsilon_{C_f}^2}. \quad (\text{A } 9)$$

We can estimate $\epsilon_{\rho_\infty/\rho}$ to a maximum of 0.7% , which is obtained from the ratio of the stagnation density and the static density at 40 m s^{-1} , but the main uncertainty comes from ϵ_{C_f} .

- (x) y_0 : this is the estimated uncertainty in the determination of the wall with respect to the centre of the Pitot tube. It is estimated from the point where the tube leaves the wall, including the precision of the tube diameter measure given by the manufacturer. The estimate of these two are 15 and $25 \mu\text{m}$, respectively. This gives an uncertainty for the position of the tube centreline of $\pm 20 \mu\text{m}$. For the different measurements in this paper, depending mainly on the free-stream velocity, the viscous length scale is within the range 10 – $45 \mu\text{m}$.
- (xi,xii) Δy : this is taken as the resolution in the y -coordinate, which is 1 and $0.5 \mu\text{m}$, respectively, for the two traverses.
- (xiii) Re_θ is calculated as

$$Re_\theta = \frac{\theta \sqrt{2\rho_\infty \Delta p_\infty}}{\mu}, \quad (\text{A } 10)$$

where we can write the expression for θ as

$$\theta = \int_0^\delta u(1-u) dy \quad (\text{A } 11)$$

and $u(y) = U(y)/U_\infty$ is the measured velocity normalized with measured free-stream velocity at distance y from the wall. The uncertainty estimate becomes

$$\epsilon_{Re_\theta} = \sqrt{\epsilon_\theta^2 + 0.25\epsilon_{\rho_\infty}^2 + 0.25\epsilon_{\Delta p_\infty}^2 + \epsilon_\mu^2}, \quad (\text{A } 12)$$

where the largest uncertainty comes from θ . The uncertainty of θ was estimated through a Monte Carlo simulation assuming random errors in the velocity measurements with the $\pm 0.3\%$ uncertainty in table 2. With the assumption of an exact free-stream value this gives us $\epsilon_{\theta MC} = \pm 0.8\%$.

- (xiv) The uncertainty for Re_{δ^*} can be determined following the same procedure as for Re_θ described above. Re_{δ^*} is used to determine the skin friction; however, owing to the logarithmic dependence, the uncertainty in C_f due to Re_{δ^*} is negligible.
- (xv) Mean velocity measured by hot-wire: the hot-wires are calibrated *in situ* in the free stream of the wind tunnel. The main uncertainty comes from the fit to the calibration curve (third-order polynomial) which is within $\pm 1.0\%$ (95% confidence interval).

REFERENCES

- CHUE, S. H. 1975 Pressure probes for fluid measurement. *Prog. Aerosp. Sci.* **16** (2), 147–223.
- DEGRAAFF, D. B. & EATON, J. K. 2000 Reynolds-number scaling of the flat-plate turbulent boundary layer. *J. Fluid Mech.* **422**, 319–346.
- DICKINSON, J. 1975 Turbulent skin friction techniques. *Tech. Rep.* Laval University, Quebec.
- GOLDSTEIN, S. 1938 Modern developments in fluid dynamics. *Proc. R. Soc. Lond.* **155**, 570–575.
- HALL, I. M. 1956 The displacement effect of a sphere in two-dimensional shear flow. *J. Fluid Mech.* **1**, 142–162.
- HITES, M. H. 1997 Scaling of high-Reynolds number turbulent boundary layers in the National Diagnostic Facility. PhD thesis, Illinois Institute of Technology.
- HOFFMAN, K. A. & CHIANG, S. T. 2000 *Computational Fluid Dynamics*, 4th edn, vol. I, Engineering Education System.
- HUTCHINS, N. & MARUSIC, I. 2007 Large-scale influences in near-wall turbulence. *Phil. Trans. R. Soc. A* **365**, 647–664.
- HUTCHINS, N., MONTY, J. P., GANAPATHISUBRAMANI, B., NG, H. C. H. & MARUSIC, I. 2011 Three-dimensional conditional structure of a high-Reynolds-number turbulent boundary layer. *J. Fluid Mech.* **673**, 255–285.
- HUTCHINS, N., NICKELS, T. B., MARUSIC, I. & CHONG, M. S. 2009 Hot-wire spatial resolution issues in wall-bounded turbulence. *J. Fluid Mech.* **635** (1), 103–136.
- LIGHTHILL, M. J. 1957 Contributions to the theory of the Pitot-tube displacement effect. *J. Fluid Mech.* **2**, 493–512.
- LIGRANI, P. M. & BRADSHAW, P. 1987 Spatial resolution and measurement of turbulence in the viscous sublayer using subminiature hot-wire probes. *Exp. Fluids* **5** (6), 407–417.
- LINDGREN, B. & JOHANSSON, A. V. 2002 Evaluation of the flow quality in the MTL wind-tunnel. *Tech. Rep.* 2002:13, Department of Mechanics, KTH, Stockholm, Sweden.
- MACMILLAN, F. A. 1954 Viscous effects on Pitot tubes at low speeds. *J. R. Aero. Soc.* **58**, 837–839.
- MACMILLAN, F. A. 1957 Experiments on Pitot tubes in shear flow. *Ministry of Supply, Aero. Res. Council* **3028**.
- MARUSIC, I. & KUNKEL, G. J. 2003 Streamwise turbulence intensity formulation for flat-plate boundary layers. *Phys. Fluids* **15** (8), 2461–2464.
- MCKEON, B. J. 2007 Pressure-based velocity measurements. In *Springer Handbook of Experimental Fluid Mechanics*, pp. 216–229. Springer.

- MCKEON, B. J., LI, J., JIANG, W., MORRISON, J. F. & SMITS, A. J. 2003 Pitot probe corrections in fully developed turbulent pipe flow. *Meas. Sci. Technol.* **14**, 1449–1458.
- MCKEON, B. J. & SMITS, A. J. 2002 Static pressure correction in high Reynolds number fully developed turbulent pipe flow. *Meas. Sci. Technol.* **13**, 1608–1614.
- METZGER, M. M., KLEWICKI, J. C., BRADSHAW, K. L. & SADR, R. 2001 Scaling the near-wall axial turbulent stress in the zero pressure gradient boundary layer. *Phys. Fluids* **13** (6), 1819–1821.
- MOCHIZUKI, S. & NIEUWSTADT, F. T. M. 1996 Reynolds-number-dependence of the maximum in the streamwise velocity fluctuations in wall turbulence. *Exp. Fluids* **21**, 218–226.
- MORRISON, J. F., MCKEON, B. J., JIANG, W. & SMITS, A. J. 2004 Scaling of the streamwise velocity component in turbulent pipe flow. *J. Fluid Mech.* **508**, 99–131.
- NICKELS, T. B., MARUSIC, I., HAFEZ, S., HUTCHINS, N. & CHONG, M. S. 2007 Some predictions of the attached eddy model for a high Reynolds number boundary layer. *Phil. Trans. R. Soc. A* **365**, 807–822.
- ÖRLÜ, R. & ALFREDSSON, P. H. 2010 On spatial resolution issues related to time-averaged quantities using hot-wire anemometry. *Exp. Fluids* **49**, 101–110.
- ÖRLÜ, R., FRANSSON, J. H. M. & ALFREDSSON, P. H. 2010 On near wall measurements of wall bounded flows: the necessity of an accurate determination of the wall position. *Prog. Aerosp. Sci.* **46**, 353–387.
- ÖSTERLUND, J. M. 1999 Experimental studies of zero pressure-gradient turbulent boundary layer flow. PhD thesis, KTH, Stockholm, Sweden.
- OZARAPOGLU, V. 1973 Measurements in incompressible turbulent flows. PhD thesis, Laval University.
- PATEL, V. C. 1965 Calibration of the Preston tube and limitations on its use in pressure gradients. *J. Fluid Mech.* **23**, 185–208.
- PERRY, A. E., HAFEZ, S. & CHONG, M. S. 2001 A possible reinterpretation of the Princeton superpipe data. *J. Fluid Mech.* **439**, 395–401.
- SCHLATTER, P. & ÖRLÜ, R. 2010 Assessment of direct numerical simulation data of turbulent boundary layers. *J. Fluid Mech.* **659**, 116–126.
- TAVOULARIS, S. 2005 *Measurement in Fluid Mechanics*. Cambridge University Press.
- TAVOULARIS, S. & SZYMCAK, M. 1989 Displacement effect of square-ended tubes in shear flows. *Exp. Fluids* **7**, 33–37.
- ZAGAROLA, M. V. & SMITS, A. J. 1998 Mean-flow scaling of turbulent pipe flow. *J. Fluid Mech.* **373**, 33–79.